HOW UNIVERSAL IS THE UNIVERSAL R-PROCESS PATTERN?

An Undergraduate Research Scholars Thesis

by

JESSICA L. MYRON

Submitted to the Undergraduate Research Scholars Program at
Texas A&M University
in partial fulfillment of the requirements for the designation as an

UNDERGRADUATE RESEARCH SCHOLAR

Approved by Research Advisor: Dr. Jennifer Marshall

May 2020

Major: Physics

TABLE OF CONTENTS

ABSTRACT

How Universal is the Universal R-Process Pattern?

Jessica Myron
Department of Physics and Astronomy
Texas A&M University

Research Advisor: Dr. Jennifer Marshall
Department of Physics and Astronomy
Texas A&M University

The rapid neutron-capture (r-)process, is responsible for the creation of about half the elements heavier than iron in the Universe. However, the nature and astrophysical site of the r-process is still strongly debated. For metal-poor stars enhanced in r-process elements ($[\mathrm{Eu/Fe}] > 0.3$), a very robust (universal) abundance pattern has been detected for the elements from Ba to Hf, matching that of the Solar system r-process abundance pattern. This project uses spectral synthesis to determine the abundance of neutron-capture elements in a sample of metal-poor stars not enhanced in Europium ($[\mathrm{Eu/Fe}] < 0.3$), to determine if this universal r-process abundance pattern extends to this group of stars and further characterize the production of neutron-capture elements in the early Universe. Answering the question how universal is the universal r-process pattern?

ACKNOWLEDGMENTS

I would like to thank my post-doc advisor Dr. Terese Hansen for her expertise, patience, and insightful comments throughout this project and written work. I would also like to thank my faculty advisor Dr. Jennifer Marshall for her guidance, advice and support for the duration of my research time at Texas A&M University.

I would also like to thank my peers, colleagues, faculty, and staff in the department of Physics and Astronomy for their warm welcome, continued moral and academic support, and advice given that I will continue to use in my future academic career. Special thanks to the Physics and Astronomy graduate students for their willingness to share their experiences and friendship making my time at Texas A&M University a positive one.

Lastly, I would like to thank my mother and father for their inspiration and encouragement in all my academic endeavors as well as my two sisters for their continued love and support.

NOMENCLATURE

EW	Equivalent Width
r-process	Rapid Neutron-Capture Process
s-process	Slow Neutron-Capture Process
ISM	Interstellar Medium
MOOG	An astronomical software package (Sobeck et al. 2011; Sneden et al. 1973)
LTE	Local Thermodynamic Equilibrium
AGB	Asypmtotic Giant Branch
NSM	Neutron Star Merger
RPA	R-Process Alliance
RAVE	RAdial Velocity Experiment

CHAPTER I

INTRODUCTION

The formation of all the elements on the periodic table is an important topic in astrophysical research. For many years there has been research about the production of heavier elements such as europium and barium, but there is still much that we don't know or understand. The neutron-capture process is responsible for the creation of these heavier elements, investigating this process in metal poor stars will probe the earlier ages of the universe and early element formation. Previous work has been done to investigate the rapid neutron-capture process (r-process) and understand a robust, universal r-process pattern. This work will attempt to understand if this universal pattern is in fact universal and allow us to better characterize the formation of heavier elements.

Chemical Abundance

Our basic understanding of elemental formation starts in the beginning of the universe, during the Big Bang where hydrogen, helium, and a little bit of lithium was created. Other so called lighter elements can be broken up into three basic categories α elements, proton capture elements, and iron peak elements [1]. α elements have even atomic numbers whose major isotopes are multiples of ^4He nucleus. Proton-capture elemental abundances are altered by hydrogen fusion reactions in the stars evolution with proton numbers $Z \leq 13$. Iron peak elements are elements from $13 \geq Z \leq 30$. The formation for elements lighter than iron ($Z = 26$) is through nuclear fusion inside a star. Nuclear fusion collides together sets of protons and neutrons, and as a result produces energy for the star. Due to nuclear physical rules, to form elements heavier than iron requires a lot of energy and force to fuse, instead of producing energy and therefore can not be created in this way. The neutron-capture process, discussed below, is responsible for the creation of the heavier elements $Z \geq 30$, and unlike the other lighter elements ($Z \leq 30$) the astrophysical sight for their formation is unknown.

Figure 1 is a periodic table showing which astronomical event created each individual

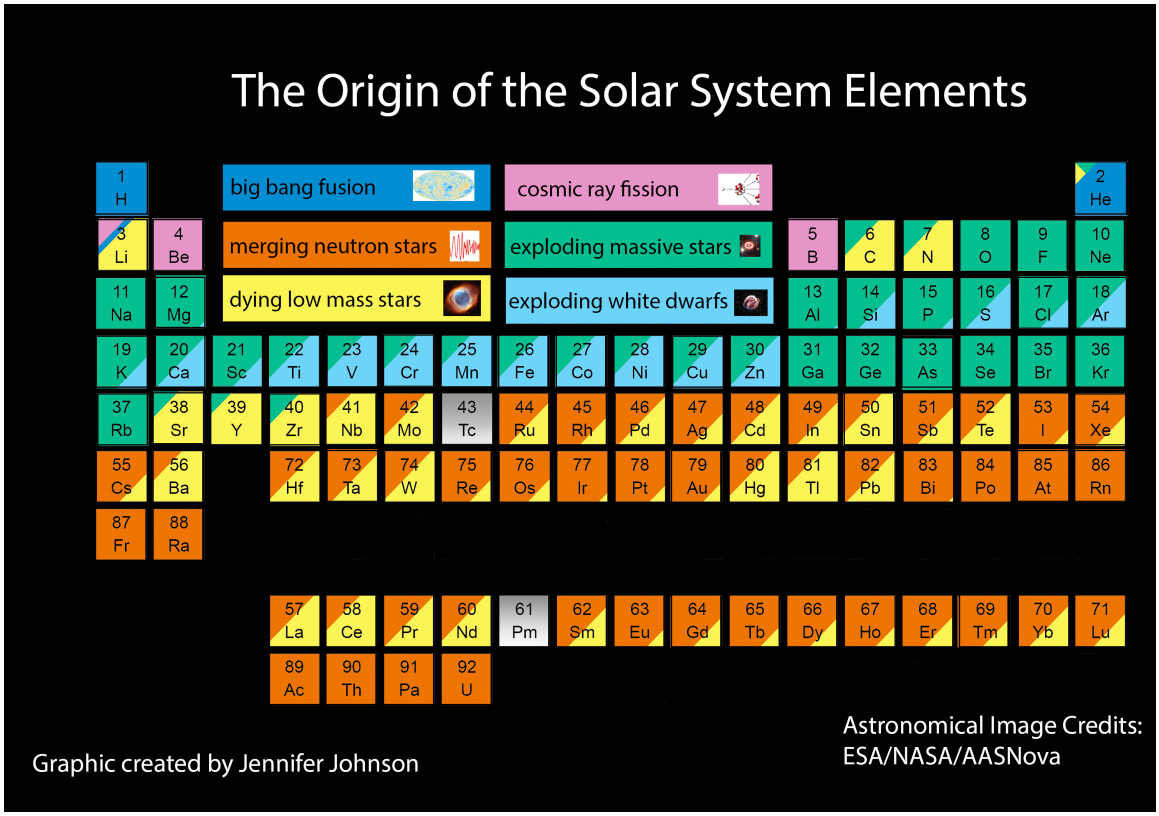

Figure 1: Periodic table indicating the astronomical origin of the Solar-system elements. [2]

element. Note that some elements can be created by more that one process, and that the area of each colored piece represents by what percent each astronomical event created these elements in the Solar-system.

Neutron-Capture Process

The neutron-capture process is a set of nuclear reactions where atomic nuclei collide with and capture neutrons. Through the process of β decay, a captured neutron decays into a proton remaining in the nucleus, an electron that escapes the nucleus, and electron neutrino [3]. Adding a proton to the nucleus, increases the atomic number to create a heavier element than before. This process can be broken up in to two basic categories, the rapid neutron-capture process (r-process) and the slow neutron-capture process (s-process). Both processes have similar formation mechanics that are well known, but about half of the elements heavier than iron are created through the r-process and the other half is through the s-process. **Figure 2** depicts the path the r- and s-

process make through known isotopes of Xe to Pr. On the right hand side of this figure indicates the elemental breakdown percentage of r- and s-process, note that some elements are created only in the r-process such as ^{136}Xe, only in the s-process such as ^{128}Xe, or a combination of both such as ^{131}Xe. The reason some isotopes are created only in the r-process is because the nuclei are being constantly bombarded with neutrons, achieving higher mass isotopes, and therefore have no stable neighbors to decay to.

In the slow neutron-capture process (s-process) the atomic nuclei have time to β decay before undergoing another neutron-capture. Time scales for neutron flux is one neutron every one thousand years, to be sufficient. It is known that the main astrophysical site for this process is in Asymptotic Giant Branch (AGB) stars. The Asymptotic Giant Branch is a region on the Hertzsprung–Russell diagram containing cool, bright, low mass stars (less than $10_{\odot}$) towards the end of their lifetime. Astronomers can directly observe this process in AGB stars and can use spectral analysis to determine the chemical abundance, learning more about the abundance patterns in relation to stellar life cycles [4]. More information is known about the s-process than the r-process because of the ability to directly observe the AGB stars.

In the rapid neutron-capture process (r-process) the atomic nuclei don't have time to β decay before capturing another neutron. Time scales for this process requires one hundred neutron-captures per second, drastically different compared to the s-process. Although we know the formation mechanics for this process there is much we don't know such as the astrophysical site or how often this happens in the universe. From what we understand about this process, a high density, high flux of neutrons is required. Prominent theoretical sights are core-collapse supernova explosions and neutron star mergers (NSMs) [5]. We can not directly observe these astrophysical sights to show the formation of the r-process because, in the case of the supernova, the spectra taken is fairly luminous and washes out the weaker abundance features making it impossible to determine chemical composition of the heavier elements. In recent years, LIGO and Virgo have identified a NSM, GW170817, that produced gravitational waves [6]. Follow-up observations of this kilonova explosion identified that the end product, multi spectrum emission of merger ejecta is

consistent with the synthesis of r-process elements [7]. Siegel et al. 2019 theorizes that the formation of these elements from, GW170817, formed in outflows of a post-merger accretion disk [8]. Although there is clear evidence for the production of r-process elements, it is unclear if NSMs are capable of producing all r-process elements or if there are multiple sites involved, the specific astrophysical site remains unknown.

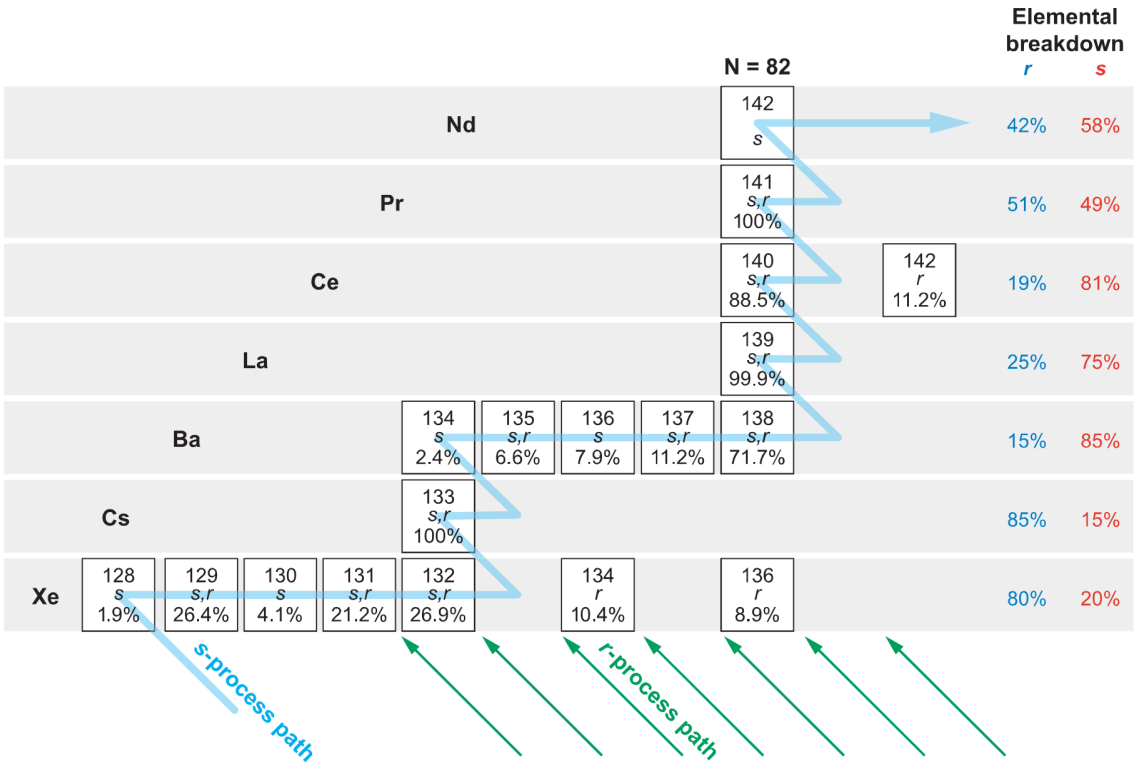

Figure 2: Chart depicting the path the r- and s-process make through known isotopes of Xe to Pr. Exception there is only one Nd isotope shown for simplicity. Elemental breakdown percentages are shown on the right hand side of this chart, note that each isotope can be created through s- or r-process only or a combination of both. The light blue line indicates the s-process path, and the black boxes indicate stable, and the green arrow-ed lines indicate the r-process path. Note the s-process path follows stable nuclei very closely going through all stable isotopes, and r-process path appears to be less stable starting from way heavier nuclei. [1]

Investigating the R-Process

How do we investigate the r-process if we can't directly observe the formation of its elements? We can do so by looking at very metal poor ($[\mathrm{Fe/H}] < -2.0$) stars. **Figure 3** shows a rudimentary progression of the universe starting from the Big Bang shown on the left. After the Big Bang the universe started cooling, enough to form hydrogen, helium, and lithium as a gas. This primordial gas collapsed and formed the first stars, called population III stars. Although these stars have not been directly observed there had to of been a first generation of stars formed, the question remains how massive were these stars and how early did they form in the universe? Population III stars are theorized to be made up of hydrogen, helium, and lithium with no contamination of heavier elements, and also theorized to be massive ($100M_{\odot} - 1,000M_{\odot}$) due to simulations of primordial gas collapses and calculations for the initial mass function [9][10][11][12]. It is known that massive stars have short life spans, only several million years, compared to smaller objects in the universe such as our Sun that has a total lifespan of ten billion years. Once these stars reach a critical low amount of hydrogen, helium is now dumped into the core and will stars burning, pushing a hydrogen-burning shell on the outer envelope of the core, and the process will continue with heavier and heavier elements. The death of population III stars result in a pair-instability supernovae explosion, which is theorized to produce heavier r-process elements, enriching the interstellar medium (ISM) surrounding it [9]. The newly produced elements are mixed with the already existing ISM gas and when this "polluted" gas collapses, it forms new stars called population II stars, that are very metal poor ($[\mathrm{Fe/H}] < -2.0$). The process to get to the first population II stars from the Big Bang takes more than three hundred million years to form, these stars are considered very old compared to the age of the universe, 13.7-billion years.

The reason we are looking at the chemical abundances of these old metal poor stars is because they would have only a few enrichment events for us to study compared to a relatively newer star, such as our Sun, that has many hundreds of thousands of enrichment events. Another reason is that since we know the s-process is created mainly in AGB stars, this process can only happen after the death of a low mass population II star, at least. This process takes approximately one

gigayear after the first enrichment events, therefore the s-process has likely little to no contribution to the elemental formation during the first few chemical enrichments.

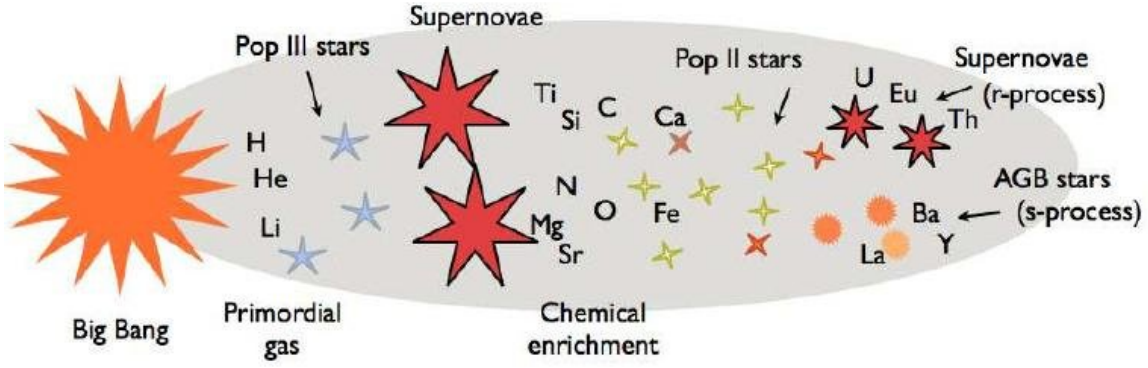

Figure 3: Credit: Prof. Anna Frabel. This diagram shows a shows a rudimentary progression of the universe since the Big Bang.[13]

Universal R-Process Pattern

The observation of an extremely metal poor star ($[\mathrm{Fe/H}] \simeq -3.12$), CS22892-052, sparked further investigation of r-process elements in metal poor stars, because of its over abundance and enrichment of heavier neutron-capture elements than ever seen before in this metallicity range [14]. This star was first discovered by the HK Objective-Prism survey with low resolution spectroscopic observations [14]. The universal r-process abundance pattern was first discovered, after further abundance analysis of this star, shown in **Figure 4** [15]. Note that all the elements on this plot fit better to the Solar r-process abundance pattern than the Solar s-process pattern.

Further investigation of this pattern is done by Sneden et al. 2003 with follow-up high resolution spectroscopic data taken from three ground based telescopes as well as the Hubble Space Telescope, for abundance analysis [17]. At this point it was unknown if star CS22892-052 was unique or if other metal poor stars followed the same scaled pattern. In 2005, Barklem produced a paper that searched for more stars with r-process enhancements through the Hamburg/ESO R-process Enhanced Stars (HERES) survey [18].

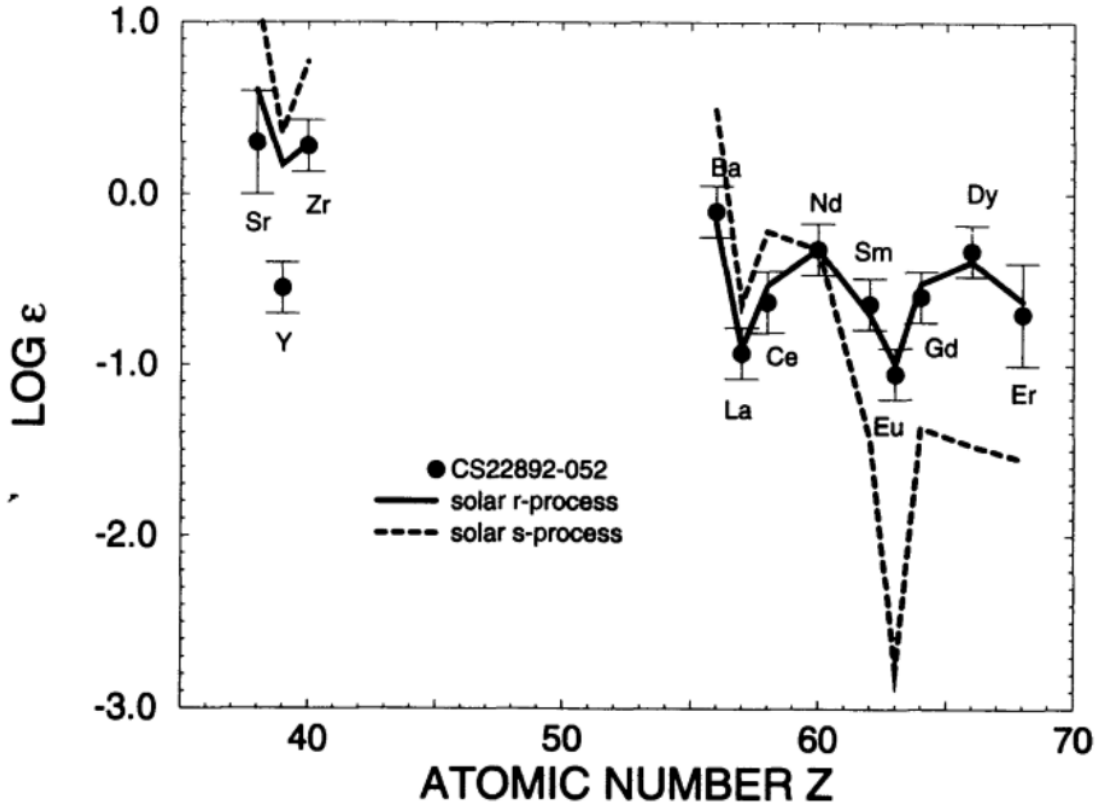

Figure 4: First plot of the universal r-process pattern. Absolute abundance values from Sneden et al. 1994 were plotted for star CS22892-052, the first star observed to have heavy neutron-capture enrichment, versus atomic number [16][15]. The abundance values are compared to theoretical determinations of the Solar r- and s-process elemental distribution from Cowan et al. 1995 indicated by the solid and dotted lines respectively [15].

Further searches for r-process enhanced stars took place across the field, Sneden et al. 2008 provided updated abundance analysis for CS22892-052 and for the Solar-system r-process abundance pattern, shown in **Figure 5** [1]. Sneden et al. 2008 also compiled updated abundance information for six r-process enhanced stars, shown in **Figure 6** plotted against the scaled Solar-system r-process abundances [1]. **Figure 6** indicated that the r-process pattern might be universal and proved that star CS22892-052 wasn't an anomaly [1]. Key information about the pattern shown in Sneden et al. 2008 is that it only matches very well to stars in the range of barium to hafnium. Also all the metal poor stars were enhanced in europium ($[\mathrm{Eu/Fe}] \geq 0.3$), considered neutron-capture rich stars [1]. The classification of neutron-capture rich stars can be split up into four main

categories r/s ($0.0 < [\mathrm{Ba/Eu}] > +0.5$), s ($[\mathrm{Ba/Fe}] > +1.0$ and $[\mathrm{Ba/Eu}] > +0.5$), r-II ($[\mathrm{Eu/Fe}] > +1.0$ and $[\mathrm{Ba/Eu}] < 0.0$), and r-I ($0.3 \leq [\mathrm{Eu/Fe}] \geq +1.0$ and $[\mathrm{Ba/Eu}] < 0.0$) [19]. Europium enhancement in a star tells us that this star had heavier elements produced predominately in the r-process. Europium is mainly produced in the r-process and is the easiest r-process dominated element to measure abundances for, this is why it is commonly used as a r-process contribution indicator in stars. For the s-process barium is an excellent indicator for heavier elements produced in the s-process, again due to how easy it is to find abundances for, compared to other s-process dominated elements.

This work looks at six stars that are not enhanced in europium, $[\mathrm{Eu/Fe}] \leq 0.3$, probing a category of stars that still have europium enrichment ($[\mathrm{Eu/Fe}] > 0.0$) meaning there is still r-process formation but not an enhancement [19]. Deriving abundances values for these six stars we then plotted it with the scaled Solar-system r-process abundance pattern to see if this pattern still matches. Answering the main question how universal is the universal r-process pattern? Does the pattern match abundances in different types of stars that produce neutron-capture elements?

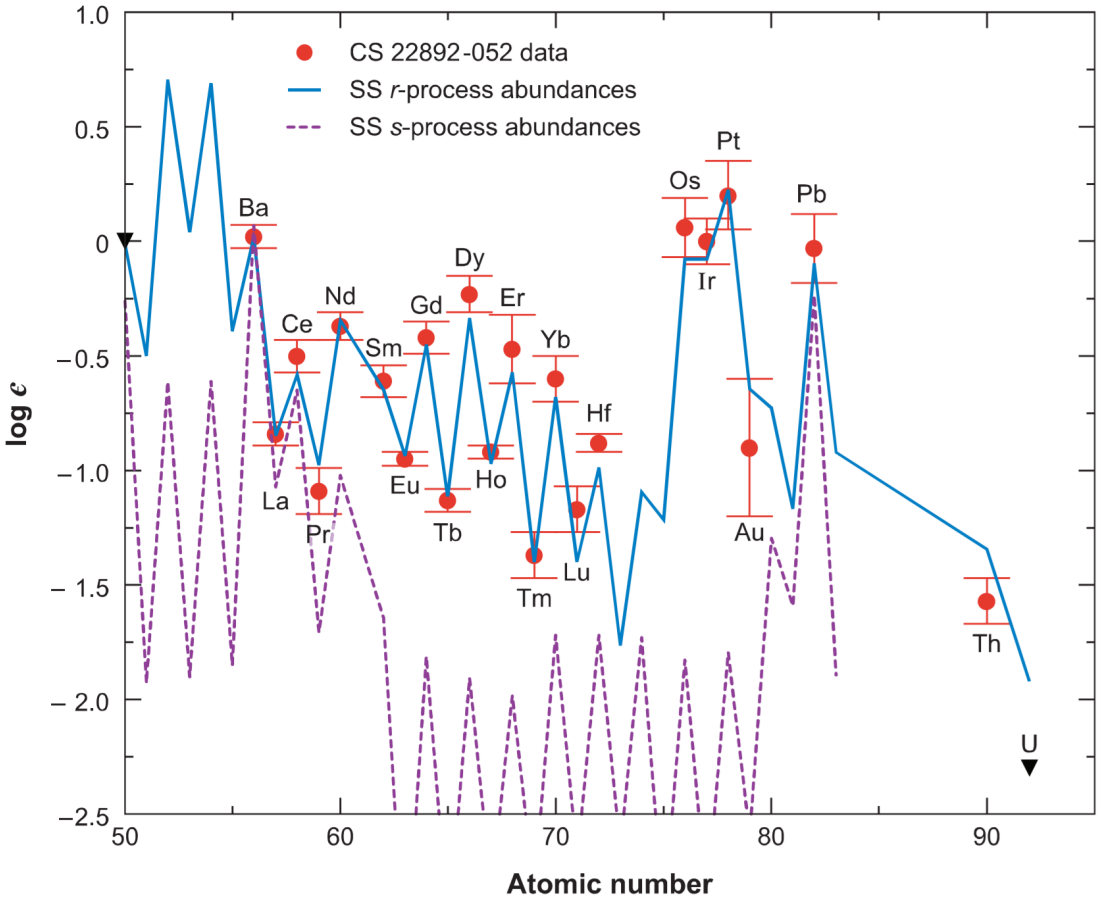

Figure 5: This plot of absolute abundance versus atomic number from Sneden et al. 2008 showing the updated universal r-process abundance pattern for the first observed metal poor ($[\mathrm{Fe/H}] \simeq -3.12$) star enhanced in neutron-capture elements, CS 22892-052 [1]. Updated abundances described in more detail in Sneden et al. 2008 [1]. The solid blue line shows the Solar-system r-process-only abundance scaled to the Europium abundance of star CS 22892-052 ($\log_\epsilon(\mathrm{Eu}) = -0.95$), and the purple dashed line is the Solar-system s-process-only abundance scaled to the Barium abundance of star CS 22892-052 ($\log_\epsilon(\mathrm{Ba}) = 0.02$) [1]. The Solar-system values are from Simmerer et al. 2004 [20]. The red points indicate the abundances for each element in star CS 22892-052. Note how well the red points match to the blue solid line.

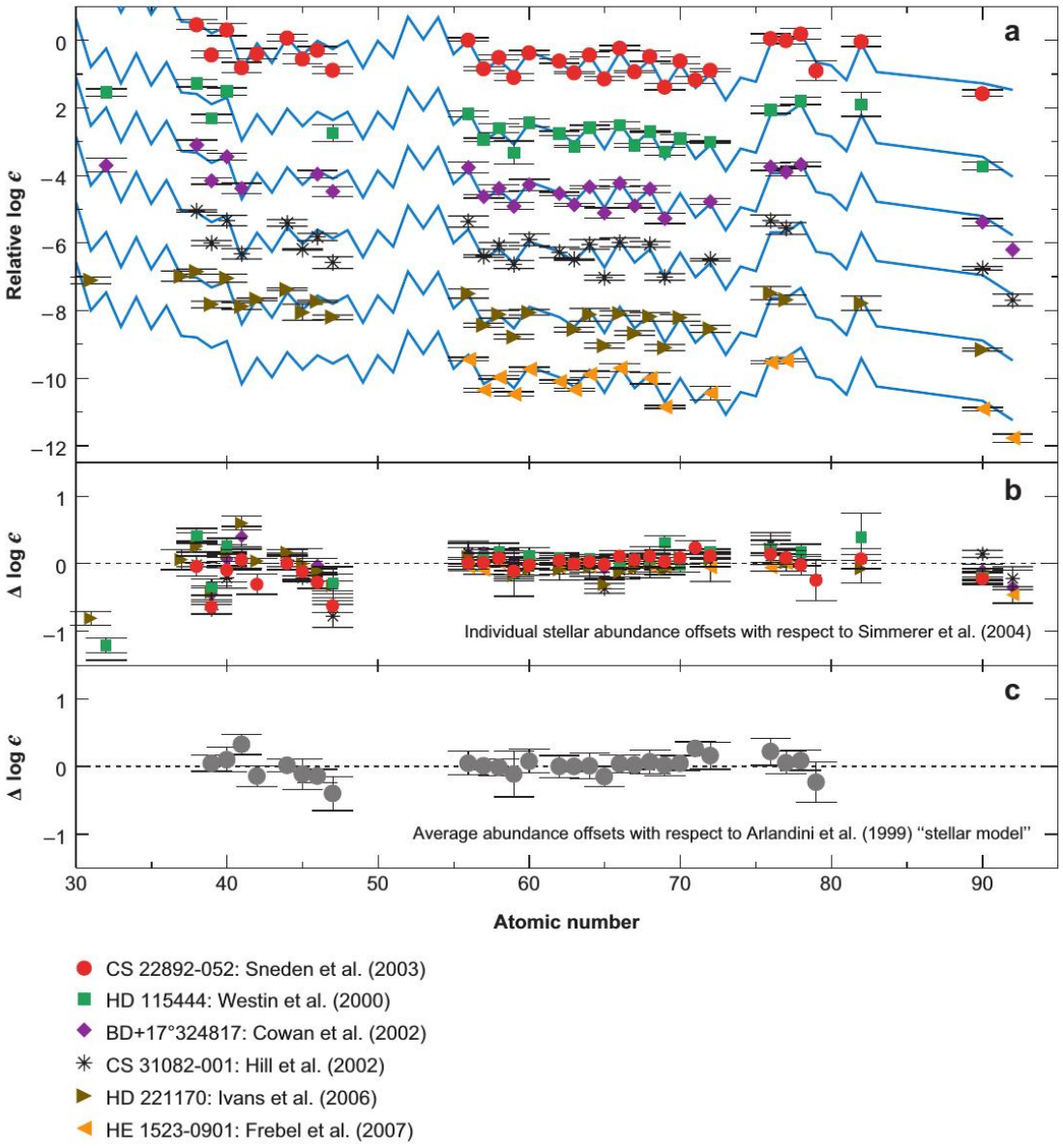

Figure 6: This plot from Sneden et al. 2008 star CS 22892-052 from **Figure 5** as well as a collection of 5 other metal poor r-process enhanced stars [1]. The abundances are compared to the Solar-system r-only abundance distribution represented by the solid blue line, scaled to the europium values of each star, listed in Sneden et al. 2008 [20][1]. (b) Shows the offsets the abundance data derived to the Solar-system data, the zero line indicates no offsets [1]. (c) Shows the average stellar abundance offsets due to scaling abundance values to the Eu value, averaging the six stars, and comparing to the Solar-system r-only distribution [1]. Note all stars except CS 22892-052 are displaced downward for convenience of the reader [1].

CHAPTER II

METHODS & DATA

Abundance Analysis

The traditional method to determine chemical abundances from absorption lines is found by using the method of Equivalent Width (EW). The Equivalent Width is the width of a rectangular area covered by the absorption feature, described in **Equation 1**:

$$EW = \int_{-\infty}^{+\infty} \frac{F_{count} - F_{\lambda}}{F_{count}} d\lambda \qquad \text{(Eq. 1)}$$

where F_{count} is the continuum flux, and F_{λ} is the line flux. Fitting an absorption line to a Gaussian profile for weak lines, Lorentz profile for strong lines, or a Voigt profile for a combination of lines results in a more accurate measurement. EW relates to the chemical abundance in **Equation 2**:

$$log(EW) = log(C) + log(N_A) + log(gf\lambda) - \theta_x \chi - log(\kappa_{\nu}) \qquad \text{(Eq. 2)}$$

where C is a constant specific for the star and quantum transition, N_A is the number of atoms in element A relative to the number of hydrogen atoms, g is the statistical weight of transition, f is the oscillator strength, $\theta_x = 5040/T$, χ is the excitation potential, and κ_{ν} is the continuum absorption coefficient. Other information is needed to determine final abundance analysis such as a model stellar atmosphere, line list information, and level populations discussed in detail in the following sections.

Spectral Synthesis

A different way to do abundance analysis, that I will be showing in this work, is spectral synthesis. Spectral synthesis is a decomposition of absorption lines in observed stellar spectrum by plotting and manipulating model spectra. Creating model spectra requires inputted information about the star such as a model stellar atmosphere and a line list with information about excitation

energy, oscillatory strength, and damping coefficients for atomic and molecular line transitions.

This method is useful compared to other traditional methods because in the observed spectra there is hyperfine structure, isotropic shifts, and element blends of several atomic and molecular lines that can cause incorrect abundance values.

Hyperfine structure or hyperfine splitting is a quantum mechanical principle due to the interaction of the electrons and proton's magnetic moments in the atom. This splitting of spectral lines is only due to odd elements interaction between the nuclear spin and angular moments of the nucleus, giving off a slightly different magnetic energy for each spin state. This effect broadens the spectral lines, and to account for these hyperfine splits we include the energy shifts in our line list (see section Line List).

The isotopic shifts are when more than one isotope for a given element contributes to the absorption lines in the stellar spectra. Each isotope has a different mass due to the different number of neutrons and this shifts the wavelength of the combined line. To account for this shift we include isotope information directly into our astronomical software package (see section Derived Abundances).

An elemental blend is when two spectral lines for different elements overlap each other and adjust the shape of said line by expanding the width and/or the dip, an example is shown in **Figure 7**. Using the traditional method the area over the spectral line doesn't account for the expanded width of the blended line, giving an incorrect value for the abundance. However, in our sample of stars elemental blending is not a big issue and doesn't affect the abundances significantly.

Derived Abundances

To derive the abundance values using spectral synthesis we used the 2017 version of MOOG, an astronomical software package [22][23]. What we see in MOOG is a spectral plot with observed data points and two synthetic spectra plotted over top. One of the synthetic spectra represents an elemental abundance of $[\mathrm{X/Fe}] = -4.5$, or little to no abundance, used as a guide to identity absorption features. The other synthetic spectra is manipulated to fit the observed spectral data points, by accounting for continuum shifts, radial velocity shifts, and fitting to a Gaussian profile.

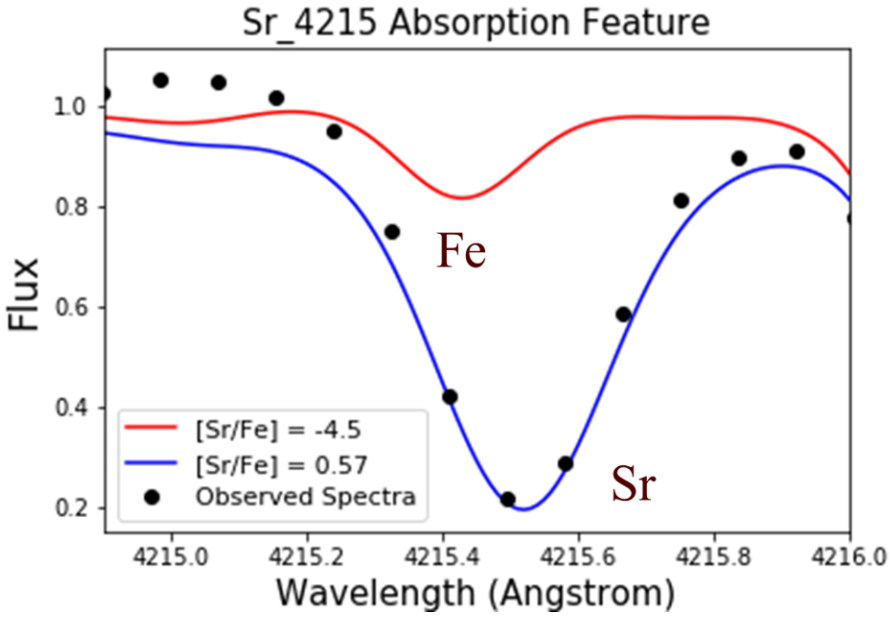

Figure 7: This plot represents the absorption feature of Strontium that has an elemental blend of iron present. The red and blue solid lines are model spectra. The red top line we input little to no abundance of Strontium or $[\mathrm{Sr/Fe}] = -4.5$, this is used as a guide to identity absorption features. The blue dipped line is what we are adjusting to fit the observed spectra from an example non-enhanced metal poor star J00021222-2241388 represented by the black points [21].

We used a Gaussian profile because we analyzed weak lines in the spectra, other fittings would use Lorentz profile for strong lines, or a Voigt profile for a combination of lines. Once we fit the synthetic spectra to the observed points the abundance of this element is outputted in terms of the ratio of that element to iron, $[\mathrm{X/Fe}]$, also known as bracket notation:

$$[\mathrm{A/B}] = \log\left(\frac{\mathrm{N(A)}}{\mathrm{N(B)}}\right)_{*} - \log\left(\frac{\mathrm{N(A)}}{\mathrm{N(B)}}\right)_{\odot} \qquad \text{(Eq. 3)}$$

where N(A) and N(B) are the column number densities for elements A and B for the star (*) and in the Sun ($\odot$) given in units per 10^{12} hydrogen atoms. An example of a derived abundance is shown in **Figure 8**, the final abundance value for yttrium in an example non-enhanced metal poor star, J00021222-2241388 is $[\mathrm{Y/Fe}] = -0.05$ [21].

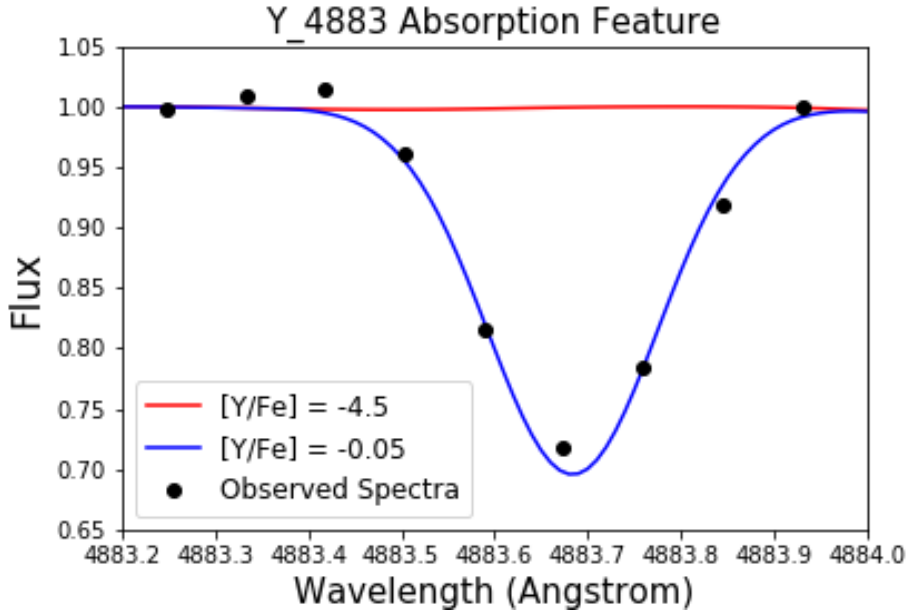

Figure 8: This plot represents the absorption feature of Yttrium. The red and blue solid lines are model spectra. The red top line has an input of little to no abundance of Yttrium or $[\mathrm{Y/Fe}] = -4.5$, used as a guide to identity absorption features. The blue dipped line is what we are adjusting to fit the observed spectra from an example non-enhanced metal poor star J00021222-2241388 represented by the black points [21].

Abundances can also be given on an absolute scale:

$$\log_{\epsilon}(\mathrm{A}) = \log(\mathrm{N(A)/N(H)}) + 12 \qquad \text{(Eq. 4)}$$

where again N(A) represents the column number density for element A and N(H) represents the column number density of hydrogen. This abundance analysis is done for many different heavier, r-process elemental lines from Sr to Hf. The main difference between the two abundance notations is that the bracket notation (**Equation 3**) is in reference to the Sun and another element (B), where as the absolute abundances (**Equation 4**) are independent of the Sun and other elements. In order to better relate our abundances values to the Solar-system r-process abundance values, we converted from bracket notation to absolute abundance, using **Equation 5**, so that our final values

are independent of the Sun and iron.

$$\log_{\epsilon}(\mathrm{A}) = [\mathrm{A/Fe}] + [\mathrm{Fe/H}] + \log_{\epsilon}(\mathrm{A})_{\odot} \quad \text{(Eq. 5)}$$

Model Stellar Atmosphere

A model stellar atmosphere is an assumption astronomers make about stellar parameters within the stellar atmosphere. Direct observation of a star's atmosphere can provide useful insite into a stellar atmosphere, but the formation of this observed spectra contains many physical variables and an accurate interpretation can't usually be made [24]. Stellar atmosphere models are needed in abundance analysis because of the difficulty to understand all physical variables when matching synthetic spectra. Stellar parameters in model atmospheres include effective temperature, gravity, metallicity ($[\mathrm{Fe/H}]$), microturbulence velocities, as well as physical particle information such as absorption coefficient, density of gas at different optical depths, and electron pressures that all effect spectral line formation.

The microturbulent velocity is defined as the gas velocity on the scale of turbulent events smaller than the mean free path of the photons. The particles in the gas of the stellar atmosphere follow the kinetic theory of gasses using the Maxwell Boltzmann distribution described in **Equation 6** as:

$$f(v) = (4\pi\frac{m}{2\pi kT})^{3/2} exp(-\frac{mv^2}{2kT})v^2 \quad \text{(Eq. 6)}$$

where m is the gas particle mass, k represents the Boltzmann constant, and T is the temperature of the gas.

The absorption coefficient is the degree light will be absorbed when traveling through the atmosphere of a star instead of being scattered or emitted. This coefficient is important to the model stellar atmosphere because this coefficient and the density of the gas determines the mean free path of the photons.

The electron pressure is important to include in the stellar atmosphere model because when the temperature of the star is large enough there is a boost of ionization and hence electron pressure.

If the temperature is hot enough it can ionize hydrogen, electron pressure is then dominated by electrons from hydrogen, in this case pressure becomes independent of chemical composition. Increasing metals in cooler atmosphere models increases the number of free electrons and the gas pressure at a given optical depth decrease with increasing metal content [24].

In this work we use an α-enhanced ATLAS9 model stellar atmosphere models [25].The stellar parameters and physical particle information gets inputted into MOOG for further abundance analysis. We use specifically an α-enhanced model because many studies of stars in the Milky Way halo establish the presence of an enhancement of α-elements and the sample of stars analyzed in this work are located in the southern hemispheres Galactic halo [26]. We would not be able to use this model in abundance analysis for a star such as the Sun, because of its location in the Milky Way disk, also because the Sun is referenced as the zero point in α-enhanced models.

In the α-enhanced model stellar atmospheres we are using, there are assumptions made about a stars physical properties, listed below:

- Assumed to have parallel plane geometry and be one dimensional, therefore the physical properties depend on one spacial coordinate, optical depth.
- Hydrostatic equlibrium
- Magnetic fields are excluded
- Stellar surface structures such as star spots or granulation are neglected.
- Local Thermodynamic Equilibrium (LTE)

Having Local Thermodynamic Equilibrium (LTE) means that the radiation of photons emitting outward of the star is the same as being re-absorbed into the star, thus creating an equilibrium. In astronomy, we know that this assumption is not necessarily true for all depths of a star. In the deeper layers of a star convection dominates which recirculates the gas and LTE is a good approximation, but this assumption breaks down in the outer layers of the star because radiative energy transport dominates and there is a flux of energy leaving the star.

Line List

Also inputted into MOOG, for abundance analysis, are generated line lists with the Linemake package [27] that gives information about wavelengths for specific elemental or molecular lines, the excitation value, and oscillatory strength. The excitation value is the amount of energy required for a spectral line to appear at a certain wavelength. We know from quantum mechanics one way to excite an electron is knowing that in atoms and molecules, electrons can absorb photons of energy of the exact same energy as a transition up or down an energy level. Other ways to excite an election included atom collisions, sometimes the energy produced in the collision can excite and electron. A low excitation value means less energy is required for that spectral line to appear and it is more likely to show up in our synthesis. The oscillatory strength gives the statistical probability that a transition will happen inside an atom. For each element the value of the oscillatory strength uses a harmonic oscillator method that compares the absorption rate of an atom to the absorption rate of a classical, single electron oscillator. Both the excitation value and oscillatory strength are useful in determining which elements are more likely to be present and useful in determining elemental blends.

Level Populations

In order to properly determine the abundance of a given element we need to account for how the population of levels depends on the temperature, T, and the effect ionization in the gas has on the spectral lines. A combination of the Saha and Boltzmann equations help us determine the abundance for a given element. The Saha equation is, shown in **Equation 7**:

$$\frac{N_{i+1}}{N_i} = \frac{2Z_{i+1}}{n_e Z_i} \left(\frac{2\pi m_e kT}{h^2} \right)^{3/2} exp(-\chi_i/kT) \qquad \text{(Eq. 7)}$$

where N_i and N_{i+1} is the number ratio of ionized to neutral atoms of a given species, χ_i is the ionization energy at a given temperature, n_e is the electron density, m_e is the electron mass, h is Planck's constant, k is Boltzmann's constant, and Z_{i+1} and Z_i are the partition functions. The

partition functions are the sum of all possible energy states in the atom, shown in **Equation 8**:

$$Z = \sum_{n=1}^{\infty} g_n exp(-(E_n - E_1)/kT) \quad \text{(Eq. 8)}$$

for a given energy level with energy E_n, where k is again Boltzmann's constant, and g_n is the statistical weight that reflects the energy degeneracy of the states. To account for the two possible spin states of the electron a 2 is placed in front of the Saha equation (**Equation 7**). The Boltzmann equation is shown in **Equation 9**:

$$\frac{N_n}{N_m} = \frac{g_n}{g_m} exp((x_n - x_m)/kT) \quad \text{(Eq. 9)}$$

where N is the ratio of populations in the two energy levels, n and m, and where x_n and x_m are the excitation energies of a given species.

Data

High resolution optical spectra was obtained, as part of the R-Process Alliance (RPA), to preform abundances analysis on our sample of stars [21]. An example of a this spectral data is shown in **Figure 9**. Data was taken in the southern hemisphere using the echelle spectrograph on du Pont 2.5 m telescope at Las Campanas Observatory, Chile [21]. The average signal to noise for the six stars analyzed is $S/N(4129\text{Å}) = 37.3$ in the wavelength range of about 3870Å-8850Å[21]. Hansen et al. 2018 investigated bright (V < 13.5), very metal-poor ([Fe/H] < -2) stars in the Milky Way halo, specifically seeking out those with heavy r-process enhancement [21]. Even though Hansen et al. 2018 refined their target star selection to be more suited to finding stars with heavy r-process enhancements (r-II stars), other types of stars were observed such r-I, limited-r, CEMP-r and other non-enhanced stars, used in this work [21]. Stellar parameters for the six non-enhanced stars analyzed, including RAdial Velocity Experiment (RAVE) ID, right ascension (RA), declination (Dec), brightness (Vmag), effective temperature (Teff), gravity (log(g)), micro-turbulent velocity (Vmicro), and metallicity ([Fe/H]) are listed in **Table 1**.

Table 1: Stellar parameters for the six stars analyzed, including RAVE ID, right ascension (RA), declination (Dec), brightness (Vmag), effective temperature (Teff), gravity (log(g)), micro-turbulant velocity (Vmicro), and metallicity ([Fe/H]).

RAVE ID	RA	Dec	Vmag	Teff (K)	log(g)	Vmicro	[Fe/H]
R074677	23h 13m 00.0s	-45° 07' 06.6"	11.2	4612	0.95	2.21	-2.64
R149535	02h 41m 21.5s	-18° 25' 37.8"	11.7	4405	0.8	1.9	-2.17
R192904	21h 51m 36.0s	-05° 43' 39.8"	10.0	4530	0.66	2.21	-2.46
R262408	00h 13m 30.7s	-12° 59' 59.4"	11.8	4405	0.5	2.6	-2.82
R288480	16h 09m 51.2s	-09° 41' 17.5"	10.5	4556	0.68	2.18	-2.82
R327190	02h 44m 14.8s	-51° 58' 24.1"	11.8	4869	1.87	1.69	-2.93

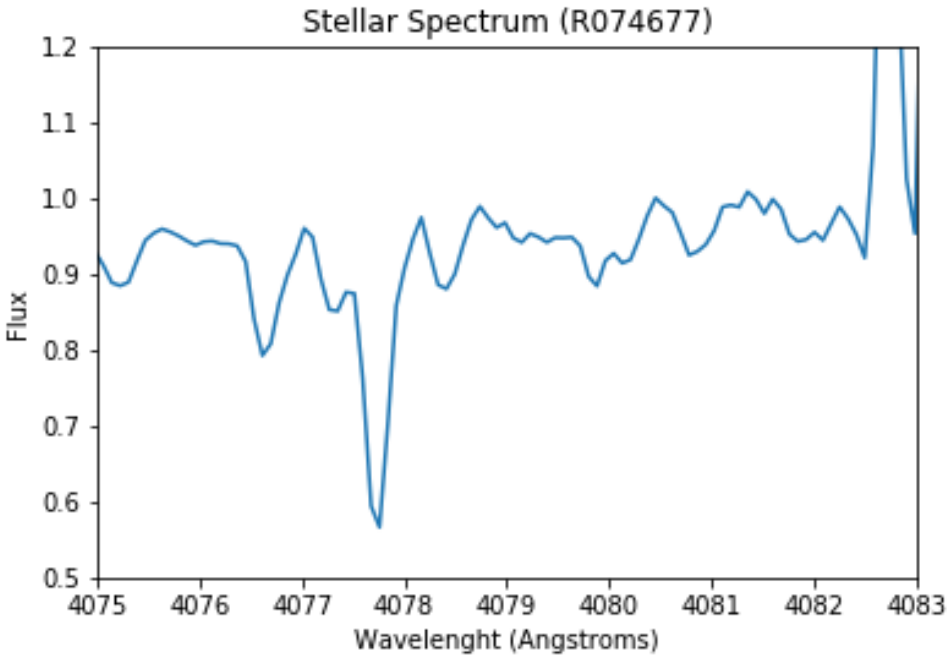

Figure 9: High resolution optical spectral data obtained as part of the R-process Alliance, for star R074677 referenced in **Table 1** [21]. This plot is zoomed in to better depict the absorption features, specifically around the strontium 4077Åline, shown by the large dip on the left-hand side. The large spike shown getting cut of on the right is cosmic interference, if an absorption line fell under one of those spikes that line was not used in final abundances calculations.

CHAPTER III

RESULTS

Final Abundances

Twelve neutron-capture elemental abundances are derived, from Sr to Dy, for six very metal poor ($[\mathrm{Fe/H}] < -2.0$), not enhanced in Europium ($[\mathrm{Eu/Fe}] < 0.3$), stars via spectral synthesis. **Tables 2-3** lists the absolute and bracket abundances for these elements in each star analyzed, also listed are the absolute Solar-system r-process abundances [28].

We plotted our abundance values and the scaled Solar-system r-process abundances versus atomic number. The Solar-system r-process abundances are derived from the total solar abundance in Asplund et al. 20009 containing both s- and r-process [28]. In order to get the r-process abundance from the Solar-system Asplund et al. 2009 subtracted out the s-process contributions [28]. The scale we used to shift the Solar-system r-process abundances are determined by taking the average difference between each derived abundance value and its corresponding Solar-system value. The final plots were replicated for all six stars analyzed, referenced in **Table 1** and depicted in **Figure 8**.

Error Analysis

Deriving abundance values from observed stellar spectrum's have multiple factors contributing to the uncertainty of each value. Two groups we will be looking at are the statistical uncertainty and systematic uncertainty.

Statistical Uncertainty

The statistical uncertainty relates to the quality of the observed stellar spectrum. To account for this we use the standard deviation of the abundances found for each elements. Some elements we were able to derive abundances for four individual lines while others we were lucky to get one clean line. To find the standard deviation values for the lucky one, standard deviation values found for elemental lines with two or more abundance derivations close to the wavelength of the lucky

Table 2: Final abundance values ([X/Fe]) and absolute abundance values ($\log_\epsilon(\mathrm{X})$) found for three of the stars referenced in **Table 1**. The Solar-system r-process absolute abundance values ($\log_\epsilon(\mathrm{X})_\odot$) are also available for comparison [28].

			R074677		R149535		R192904	
Element	Z	$\log_\epsilon(\mathrm{X})_\odot$	[X/Fe]	$\log_\epsilon(\mathrm{X})$	[X/Fe]	$\log_\epsilon(\mathrm{X})$	[X/Fe]	$\log_\epsilon(\mathrm{X})$
Sr	38	1.95	-1.54	-2.23	0.35	0.13	-0.70	-1.21
Y	39	1.66	-0.50	-1.48	0.00	-0.51	-0.70	-1.50
Zr	40	1.85	-0.23	-1.02	...	...	-0.60	-1.21
Ba	56	1.45	-0.53	-1.72	0.37	-0.35	-0.10	-1.11
La	57	0.58	0.20	-1.86	0.10	-1.49	-0.24	-2.12
Ce	58	0.85	-0.15	-1.94	...	...	-0.18	-1.79
Pr	59	0.45	0.20	-1.99	0.00	-1.72	-0.03	-2.03
Nd	60	1.09	-0.15	-1.70	0.13	-0.96	-0.18	-1.55
Sm	62	0.78	0.10	-1.76	-0.25	-1.64	...	...
Eu	63	0.49	0.25	-1.90	0.21	-1.47	0.03	-1.94
Gd	64	0.98	0.25	-1.66	0.15	-1.04	-0.23	-1.71
Dy	66	1.10	0.00	-1.54	0.20	-0.87	0.23	-1.14

Table 3: Final abundance values ([X/Fe]) and absolute abundance values ($\log_\epsilon(\mathrm{X})$) found for the other three stars referenced in **Table 1**. The Solar-system r-process absolute abundance values ($\log_\epsilon(\mathrm{X})_\odot$) are also available for comparison [28].

			R262408		R288480		R327190	
Element	Z	$\log_\epsilon(\mathrm{X})_\odot$	[X/Fe]	$\log_\epsilon(\mathrm{X})$	[X/Fe]	$\log_\epsilon(\mathrm{X})$	[X/Fe]	$\log_\epsilon(\mathrm{X})$
Sr	38	1.95	-0.33	-1.20	-0.50	-1.37	-0.50	-1.48
Y	39	1.66	-0.50	-1.66	-0.45	-1.61	-0.27	-1.54
Zr	40	1.85	0.00	-0.97	-0.02	-0.99	0.10	-0.98
Ba	56	1.45	-0.53	-1.90	-0.29	-1.66	-0.83	-2.31
La	57	0.58	-0.18	-2.42	-0.17	-2.41	0.43	-1.92
Ce	58	0.85	0.25	-1.73	0.13	-1.84	0.63	-1.46
Pr	59	0.45	...	...	0.30	-2.07	0.75	-1.73
Nd	60	1.09	-0.15	-1.88	0.13	-1.61	0.55	-1.29
Sm	62	0.78	...	...	0.10	-1.94	0.40	-1.75
Eu	63	0.49	0.00	-2.33	-0.03	-2.36	0.13	-2.31
Gd	64	0.98	...	...	...	...	1.13	-1.08
Dy	66	1.10	0.18	-1.72	0.13	-1.72	0.87	-1.83

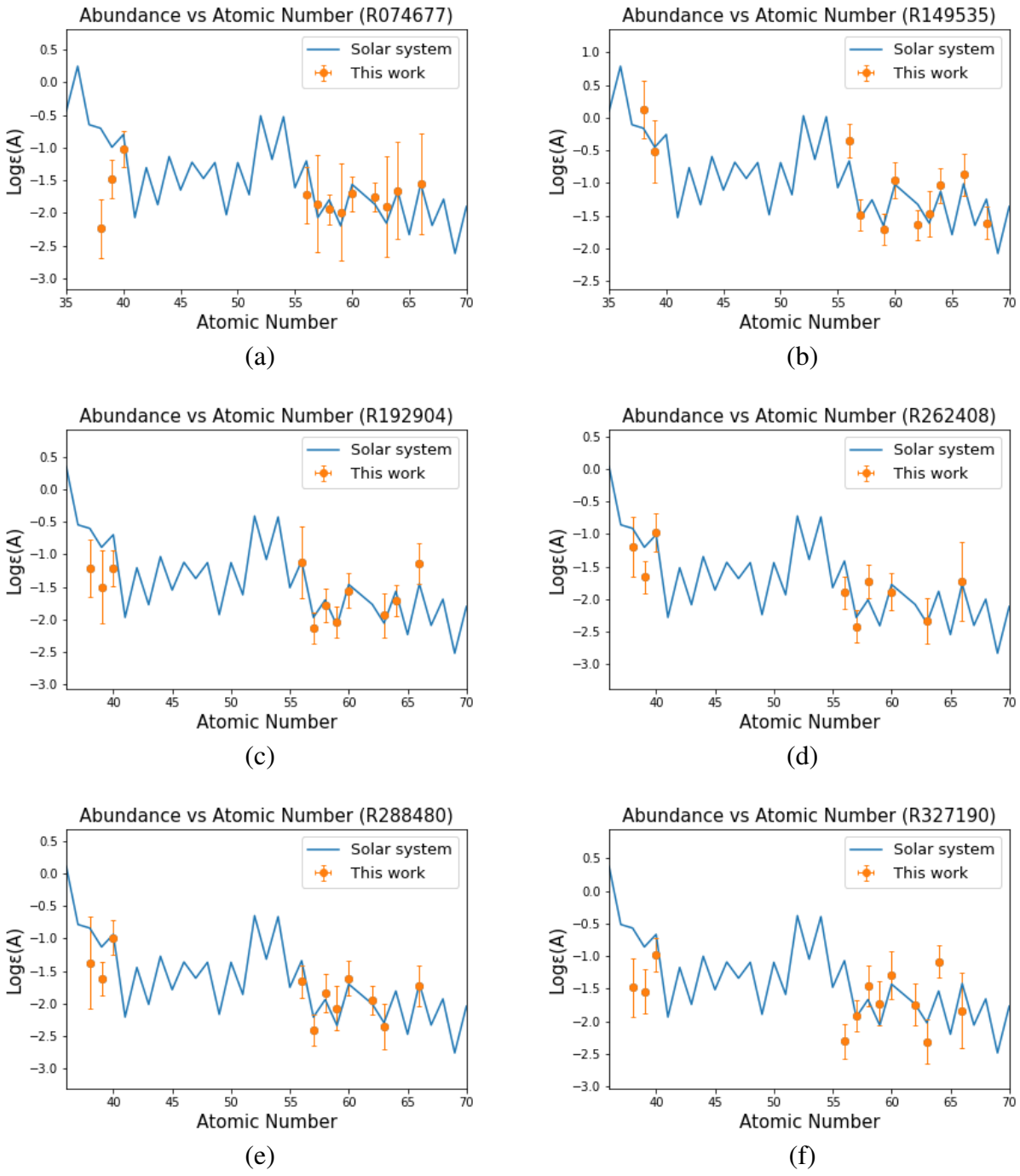

Figure 10: Elemental abundance values for six different metal poor stars not enhanced in europium ($[\mathrm{Eu/Fe}] < 0.3$), represented by the orange points, plotted against the Solar-system r-process abundance values, represented by the solid blue line. The universal r-process pattern is in the range of Ba (56) to Dy (66) on the right hand side of each plot.

Table 4: Standard deviation values for each elemental abundance found in all six stars observed, referenced in **Table 1**.

	R074677	R149535	R192904	R262408	R288480	R327190
$\sigma_{stat,[\mathrm{Sr/Fe}]}$	0.07	0.05	0.06	0.13	0.55	0.08
$\sigma_{stat,[\mathrm{Y/Fe}]}$	0.15	0.41	0.5	0.03	0.09	0.24
$\sigma_{stat,[\mathrm{Zr/Fe}]}$	0.07	...	0.08	0.13	0.08	0.05
$\sigma_{stat,[\mathrm{Ba/Fe}]}$	0.36	0.05	0.5	0.07	0.05	0.13
$\sigma_{stat,[\mathrm{La/Fe}]}$	0.70	0.07	0.06	0.11	0.05	0.08
$\sigma_{stat,[\mathrm{Ce/Fe}]}$	0.05	...	0.13	0.11	0.21	0.23
$\sigma_{stat,[\mathrm{Pr/Fe}]}$	0.70	0.07	0.08	...	0.26	0.25
$\sigma_{stat,[\mathrm{Nd/Fe}]}$	0.05	0.09	0.02	0.11	0.05	0.24
$\sigma_{stat,[\mathrm{Sm/e}]}$	0.05	0.09	...	...	0.05	0.24
$\sigma_{stat,[\mathrm{Eu/Fe}]}$	0.70	0.13	0.08	0.13	0.10	0.08
$\sigma_{stat,[\mathrm{Gd/Fe}]}$	0.70	0.13	0.07	...	...	0.09
$\sigma_{stat,[\mathrm{Dy/Fe}]}$	0.70	0.07	0.02	0.53	0.03	0.48

one line is used in both results. The standard deviation for each element in each star is shown in **Table 4**.

Systematic Uncertainty

The systematic uncertainty relates to the stellar parameters included in the synthesis of the model spectra. Each parameter, if changed would effect the model spectral in a different way, too account for these changes one would go in and re-derive abundances using perturbed atmosphere models. Using **Equations 10-13** is how you derive the effect each stellar parameter has on the abundance values. X represents each element and $[\mathrm{X/Fe}]_{Teff}$ represents the abundance shifted by a warmer or colder atmosphere model, etc. To find the total systematic uncertainty, add each offset in quadrature shown in **Equation 14**. The final calculations are listed in **Table 5** for one star, these

Table 5: Star R074677 abundance change per element due to parameter uncertainty. σ_{Teff} represents the spectral abundance offset for a change in effective temperature, $\sigma_{\log(g)}$ is the change due to gravity, σ_{Vmicro} is the change due to microturbulant velocities, $\sigma_{[\mathrm{Fe/H}]}$ is the change due to metallicity, and σ_{sys} is the final systematic uncertainty value for each elemental abundance.

	δ_{Teff}	$\delta_{\log(g)}$	δ_{Vmicro}	$\delta_{[\mathrm{Fe/H}]}$	σ_{sys}
[Sr/Fe]	0.33	0.05	0.21	0.20	0.44
[Y/Fe]	0.10	0.10	0.10	0.18	0.25
[Zr/Fe]	0.14	0.08	0.00	0.21	0.26
[Ba/Fe]	0.07	0.05	0.00	0.22	0.24
[La/Fe]	0.12	0.00	0.03	0.19	0.23
[Ce/Fe]	0.09	0.08	0.00	0.19	0.22
[Pr/Fe]	0.15	0.04	0.02	0.17	0.23
[Nd/Fe]	0.19	0.10	0.05	0.15	0.27
[Sm/Fe]	0.10	0.03	0.00	0.18	0.21
[Eu/Fe]	0.23	0.09	0.10	0.19	0.33
[Gd/Fe]	0.13	0.07	0.04	0.17	0.23
[Dy/Fe]	0.20	0.13	0.09	0.18	0.31

offsets can be assumed for the other five stars in our sample.

$$\delta_{Teff} = [\mathrm{X/Fe}]_{orig.} - [\mathrm{X/Fe}]_{Teff} \quad \text{(Eq. 10)}$$

$$\delta_{Log(g)} = [\mathrm{X/Fe}]_{orig.} - [\mathrm{X/Fe}]_{Log(g)} \quad \text{(Eq. 11)}$$

$$\delta_{Vmicro} = [\mathrm{X/Fe}]_{orig.} - [\mathrm{X/Fe}]_{Vmicro} \quad \text{(Eq. 12)}$$

$$\delta_{[\mathrm{Fe/H}]} = [\mathrm{X/Fe}]_{orig.} - [\mathrm{X/Fe}]_{[\mathrm{Fe/H}]} \quad \text{(Eq. 13)}$$

$$\sigma_{sys} = \sqrt{\delta^2_{Teff} + \delta^2_{\log(g)} + \delta^2_{Vmicro} + \delta^2_{[\mathrm{Fe/H}]}} \quad \text{(Eq. 14)}$$

Final Uncertainty

The final uncertainty, which is the length of the error bars in **Figure 8**, can be calculated as such in **Equation 15**, and the final values are expressed in **Table 6**.

$$\sigma_{tot} = \sqrt{\sigma^2_{stat} + \sigma^2_{sys}} \quad \text{(Eq. 15)}$$

Table 6: Final uncertainties calculated for each element found in each of the six stars referenced in **Table 1**. These final values represent the error bars in **Figure 8**.

	R074677	R149535	R192904	R262408	R288480	R327190
$\sigma_{tot,Sr}$	0.45	0.44	0.44	0.46	0.70	0.45
$\sigma_{tot,Y}$	0.29	0.48	0.56	0.25	0.26	0.34
$\sigma_{tot,Zr}$	0.27	0.26	0.27	0.29	0.27	0.26
$\sigma_{tot,Ba}$	0.43	0.25	0.55	0.25	0.25	0.27
$\sigma_{tot,La}$	0.74	0.24	0.24	0.25	0.24	0.24
$\sigma_{tot,Ce}$	0.23	0.22	0.26	0.25	0.30	0.31
$\sigma_{tot,Pr}$	0.74	0.24	0.24	0.23	0.34	0.34
$\sigma_{tot,Nd}$	0.27	0.28	0.27	0.29	0.27	0.36
$\sigma_{tot,Sm}$	0.22	0.23	...	...	0.22	0.32
$\sigma_{tot,Eu}$	0.77	0.35	0.34	0.35	0.35	0.34
$\sigma_{tot,Gd}$	0.74	0.26	0.24	0.23	0.23	0.25
$\sigma_{tot,Dy}$	0.77	0.32	0.31	0.61	0.31	0.57

Discussion

Outside of the universal r-process abundance pattern, we derived abundances for strontium, yttrium, and zirconium. On the left hand side of **Figure 10** we plotted the absolute abundances compared to the Solar-system r-process abundances. We looked at these elements because they are considered lighter neutron-capture elements, predominately produced in the s-process, but also contribute to the r-process pattern. These elements specifically has stronger absorption features compared to other lighter neutron-capture elements in our wavelength range. About half of these abundance values fit within the error bars, and it is worth noting that these elements fall predominately at or below the Solar-system r-process abundance line. This isn't surprising since a r-process pattern doesn't emerge outside of the universal range, Ba to Hf.

Universal R-process Pattern

The final absolute abundance results for twelve neutron-capture elements, from Sr to Dy, in six stars are plotted in relation to the universal r-process pattern, from Ba to Hf, **Figure 10**. **Figure 10** shows that for most of the absolute abundances for elements from Ba to Hf, seem to fit the universal r-process pattern and is with in the error bars. There are a few exceptions but two more obvious deviations to the error bar fit, is barium (Z=56) and Gadolinium (Z=64)

in **Figure 10(f)**. This particular star, R327190, has the lowest absolute abundance for barium of ($\log_\epsilon(Ba) = -2.31$) and highest absolute abundance for gadolinium ($\log_\epsilon(Gd) = -1.08$), compared to the other elements analyzed in this star. Knowing that barium is mostly produced in the s-process, having a lower abundance value derived for this star should indicate that this star has less of the s-process contributed to the formation of elements. Therefore the r-process abundance pattern should fit well for all points, but the opposite is observed. A possible explanation is that the weak s-process could have played a part in the formation of the elements in this star. The weak s-process has a different neutron source than the normal s-process and is produced in the He burning core of massive stars. These massive stars are consistent with the time scales of the formation of the first r-process elements in the universe and can not be ruled out as a production source. Future work could contain double checking the abundance value in this work, and investigating the weak s-process contributions.

We were only able to analyze the spectral data for six stars, this is not enough to come to a meaningful conclusion about the universality of the r-process abundance pattern, but we can still look at the results and make observations. A tentative conclusion from this small sample of stars indicates that the universal r-process pattern is in fact universal. Assuming the pattern is universal for all types of stars, what does that tell us about the r-process?

In physics we know that certain parameters can effect the state of a gas, things like temperature, pressure, neutron flux, and velocity of ejected materials that depend on each other. If these thermodynamical properties are dependent on the universal r-process pattern then all astrophysical sites must produce the same pattern. Therefore all explosion mechanisms, for astrophysical sites, must produce the r-process elements in the same way. Knowing the constraints for the formation of these heavier r-process elements will help astronomers better identify other candidates for astrophysical sites, and rule out other theorized sites, if certain conditions can not be met.

R-process Pattern Pollution

Discussed in the subsection above, the weak s-process could influence or "pollute" the r-process pattern in the metal poor stars. Unlike the normal s-process, the weak s-process has

a different neutron source. Both processes are a result of He burning in the core of their star during the last stages of its lifespan, but the weak s-process is found in dying massive stars and the normal s-process is found in dying low mass stars. We know from the introduction that the r-process happens first in the time scale of the universe compared to the s-process by about one gigayear. Higher mass stars evolve off the main sequence more quickly than low mass star due to the amount of energy needed to keep the star fusing. These massive stars could evolve around the same timescales as the production of the first few r-process enrichment events. Although the normal s-process should have little to no interference in the r-process pattern, and since the weak s-process can be found around the same time scales as the first r-process enrichment events, we can not rule out the weak s-process contribution to similar r-process elements produced in the early universe. We can also not be certain that the star we are analyzing is part of the very first generation of r-process enriched stars, therefore we can also not rule out the normal s-process entirely. For future work, one could look into the influence of the normal/weak s-process by subtracting out known contributions. Plotting the new r-process only abundance values could potentially confirm the universality of the r-process pattern or show no correlation.

CHAPTER IV

SUMMARY

Twelve neutron-capture elemental abundances, from Sr to Dy, are derived for six metal poor ($[\mathrm{Fe/H}] < -2.0$), not enhanced in europium ($[\mathrm{Eu/Fe}] < 0.3$), stars via spectral synthesis. We were only able to analyze the spectral data for six stars, to compare with the universal r-process abundance pattern, from Ba-Hf, in **Figure 10**. Six stars is not enough to come to a meaningful conclusion about the universality of the r-process abundance pattern, but we can still make some observations from the data produced.

Figure 8 shows the final plot comparing the absolute abundances for our six stars and the Solar-system r-process absolute abundances versus atomic number. The tentative conclusion from these graphs indicates that the universal r-process pattern is universal, due to how well the data fits with in the error bars. Other evidence I used is from previous work done with europium enhanced stars ($[\mathrm{Eu/Fe}] > 0.3$) shown in **Figure 5** that indicated how well the pattern should fit to give them the confirmation that this pattern held for their sample of stars [1]. To reach a more sound conclusion more stars would need to be analyzed, potentially in different metal poor metallicity ranges. The RPA is doing just that by continuing their work investigating the r-process and hopefully be able to collect observations for a wide variety of metal poor stars in the Milky Way halo. Other future work includes investigating the weak s-process contribution to abundances derived for the r-process.

REFERENCES

[1] C. Sneden, "Neutron-capture elements in the early galaxy," *Annual Review of Astronomy and Astrophysics*, vol. 46, p. 241, 2008.

[2] "Origin of the elements in the solar system." Credit: Jennifer Johnson, Web, 2017.

[3] E. M. Burbidge, "Synthesis of the elements in stars," *Reviews of Modern Physics*, vol. 29, p. 547, 1957.

[4] F. K*ä*ppeler, "The *s* process: Nuclear physics, stellar models, observations," *Reviews of Modern Physics*, vol. 83, p. 157, 2011.

[5] J. Cowan, "Making the heaviest elements in the universe: A review of the rapid neutron capture process," *Reviews of Modern Physics*, arXiv:1901.01410, 2019.

[6] B. P. Abbott, "Gw170817: Observation of gravitational waves from a binary neutron star inspiral," *Physical Review Letters*, vol. 119, p. 161101, 2017.

[7] C. Kilpatrick, "Swope supernova survey 2017a (sss17a), the optical counterpart to a gravitational wave source," *Science*, vol. 358, pp. 1556–1558, 2017.

[8] D. Siegel, "Gw170817–the rst observed neutron star merger and its kilonova: implications for the astrophysical site of the r-process," *The European Physical Journal A*, vol. 55, no. 11, 2019.

[9] N. Y. G. Jeremiah P. Ostriker, "Reheating of the universe and population iii," *The Astrophysical Journal Letters*, vol. 472, no. 2, 1996.

[10] P. S. C. Volker Bromm and R. B. Larson, "Forming the first stars in the universe: The fragmentation of primordial gas," *The Astrophysical Journal Letters*, vol. 527, no. 1, 1999.

[11] M. L. N. Tom Abel, Greg L. Bryan, "The formation and fragmentation of primordial molecular clouds," *The Astrophysical Journal*, vol. 540, pp. 39–44, 2000.

[12] M. U. Fumitaka Nakamura, "On the initial mass function of population iii stars," *The Astophysical Journal*, vol. 548, no. 1, 2001.

[13] "Stellar cycle." Credit: Prof. Anna Frabel, Web.

[14] S. S. T. Beers, G. Preston, "A search for stars of very low metal abundance. ii," *The Astronomical Journal*, vol. 103, no. 6, pp. 1987–2034, 1992.

[15] J. Cowan, "Evidence of heavy element nucleosynthesis early in the history of the galaxy: The ultra-metal-poor stars cs 22892-052," *The Astrophysical Journal*, vol. 439, pp. L51–L54, 1995.

[16] C. Sneden, "Ultrametal-poor halo stars: The remarkable spectrum of cs 22892-052," *The Astrophysical Journal*, vol. 431, no. 1, pp. L27–L30, 1994.

[17] C. Sneden, "The extremely metal-poor, neutron capture-rich star cs 22892-052: A comprehensive abundance analysis," *The Astrophysical Journal*, vol. 591, no. 2, p. 936–953, 2003.

[18] P. S. Barklem, "The hamburg/eso r-process enhanced star survey (heres) ii. spectroscopic analysis of the survey sample," *Astronomy and Astrophysics*, vol. 439, pp. 129–151, 2005.

[19] N. C. Timothy C. Beers, "The discovery and analysis of very metal-poor stars in the galaxy," *Annual Review of Astronomy and Astrophysics*, vol. 43, pp. 531–580, 2005.

[20] J. Simmerer, "The rise of the s-process in the galaxy," *The Astrophysical Journal*, vol. 617, no. 2, p. 1091, 2004.

[21] T. Hansen, "The r-process alliance: First release from the southern search for r-process-enhanced stars in the galactic halo," *The Astrophysical Journal*, vol. 858, p. 92, 2018.

[22] J. Sobeck, "The abundances of neutron-capture species in the very metal-poor globular cluster m15: A uniform analysis of red giant branch and red horizontal branch stars," *The Astronomical Journal*, vol. 141, no. 6, p. 175, 2011.

[23] C. Sneden *Thesis (PH.D.)–THE UNIVERSITY OF TEXAS AT AUSTIN*, vol. 35-01, sec. B, p. 0028, 1973.

[24] D. F. Gray, *The Observation and Analysis of Stellar Photospheres, Third Edition*. Cambridge University Press, 2005.

[25] L. Sbordone, "Atlas and synthe under linux," *Memorie della Società Astronomica Italiana Supplementi (Italian)*, vol. 5, p. 93, 2004.

[26] X. Fu, "New parsec database of -enhanced stellar evolutionary tracks and isochrones i. calibration with 47 tuc (ngc104) and the improvement on rgb bump," *Monthly Notices of the Royal Astronomical Society*, vol. 476, no. 1, p. 496–51, 2018.

[27] C. Sneden priv. comm.

[28] M. Asplund, "The chemical composition of the sun," *Annual Review of Astronomy and Astrophysics*, vol. 47, p. 481, 2009.